Unrestricted absolutely localized molecular orbitals for energy decomposition analysis: Theory and applications to intermolecular interactions involving radicals

Paul R. Horn, Eric Jon Sundstrom, Thomas A. Baker, and Martin Head-Gordon

Citation: The Journal of Chemical Physics **138**, 134119 (2013); doi: 10.1063/1.4798224
View online: http://dx.doi.org/10.1063/1.4798224
View Table of Contents: http://aip.scitation.org/toc/jcp/138/13
Published by the American Institute of Physics

Unrestricted absolutely localized molecular orbitals for energy decomposition analysis: Theory and applications to intermolecular interactions involving radicals

Paul R. Horn,[1,a)] Eric Jon Sundstrom,[1] Thomas A. Baker,[1] and Martin Head-Gordon[1,2]
[1]*Department of Chemistry, University of California, Berkeley, Berkeley, California 94720, USA*
[2]*Chemical Sciences Division, Lawrence Berkeley National Laboratory, Berkeley, California 94720, USA*

(Received 25 December 2012; accepted 28 February 2013; published online 5 April 2013)

Radical-closed shell and radical-radical intermolecular interactions are less well-understood than those between closed shell species. With the objective of gaining additional insight, this work reports a generalization of the absolutely localized molecular orbital (ALMO) energy decomposition analysis (EDA) to open shell fragments, described by self-consistent field methods, such as standard density functional theory. The ALMO-EDA variationally partitions an intermolecular interaction energy into three separate contributions; frozen orbital interactions, polarization, and charge transfer. The first examples involve comparison of the interactions of alkanes and alkyl radicals (methyl radical, methane, tertiary butyl radical, and isobutane) with sodium, potassium, hydronium, and ammonium cations. A second series of examples involve benzene cation interacting with a series of nucleophiles in both on-top and side-on geometries. The ALMO-EDA yields a variety of interesting insights into the relative roles of its component contributions as the interacting partners and their geometries are changed. © *2013 American Institute of Physics*. [http://dx.doi.org/10.1063/1.4798224]

I. INTRODUCTION

The idea that one can take a molecule or, more generally, a fragment consisting of one or more atoms, which is understood in one chemical environment (such as a dilute gas) and make arguments about the effect of placing that fragment in another chemical environment by performing a sort of qualitative perturbation theory is central to chemistry. To facilitate this process, chemists have developed several ways to describe and categorize the interactions that are most important to the perturbation such as permanent electrostatics, polarization, charge transfer, and dispersion; however, when the interacting systems become complex, it can become difficult to understand intuitively which are the most relevant modes of interaction. Energy decomposition analysis (EDA) provides a way of quantifying the significance of the different modes of interaction by dividing the total binding energy into energy contributions from each. However, since there are no clearly defined operators corresponding to, for instance, the energy lowering due to the polarization of a molecule, the criteria by which EDA schemes should be judged are that the components be physically meaningful, efficiently calculable, and, to a lesser extent, theoretically satisfying.

To this end, many energy decomposition schemes have been proposed in the literature with varying levels of success. The popular Symmetry Adapted Perturbation Theory (SAPT) provides a means of calculating the total intermolecular interaction and also, by binning different terms in the expansion, can attribute all portions of the computed interaction energy to different physical contributions.[1–11] The SAPT calculated interaction energy can agree quite well with higher levels of theory, and the SAPT methods are computationally less expensive than the higher level of theory that they attempt to reproduce. However, SAPT calculations are generally also more expensive than standard self-consistent field (SCF) calculations. Another method that aims to calculate intermolecular interactions by taking advantage of a fragment scheme but with considerably lower cost is the well established effective fragment potential (EFP) method.[12–15] Another approach based on a different type of perturbation theory is the Natural Energy Decomposition Analysis (NEDA) method,[16–18] which draws considerably from both the framework and the interpretation of Natural Bonding Orbitals (NBOs).[19] NBO and NEDA methods have proved tremendously valuable for elucidating *trends* across intermolecular interactions in diverse systems. However, caution is required in interpreting NBO/NEDA energy contributions quantitatively. Like NBO, the NEDA scheme is based on perturbation theory, and yields an unlikely result, that charge transfer contributions are larger than the total interaction energy, for even weakly interacting systems such as water.[18]

Alternatively, many methods calculate variationally optimized intermediate wave functions, beginning with the Kitaura and Morokuma (KM) EDA[20] for Hartree-Fock (HF) theory, and the Ziegler-Rauk approach for the Xα method.[21–23] There have been many subsequent implementations and improvements to these methods.[24–27] One noteworthy evolution of the KM-EDA is the variational evaluation of a polarization by using a fragment-blocked molecular orbital coefficient matrix[28,29] to define an intermediate energy associated with polarization. This approach is employed in the block-localized wave function (BLW)-EDA,[28,30–32] and the Absolutely Localized MO (ALMO)-EDA (discussed in more detail below). It should be noted that this way of calculating

a)Electronic mail: prhorn@berkeley.edu. Telephone: 510-642-5957. Fax: 510-643-1255

polarization contributions is similar to the method employed by Sadlej[33] for the calculation of induction interactions for non-overlapping subsystems.

Another method is the density based scheme of Wu *et al.*,[34] which variationally optimizes the energy given a grid based charge constraint. Wu *et al.*[34] construct an initial total system density that is a sum of fragment densities by searching for the corresponding minimum energy antisymmetric wavefunction; however, during this procedure, the orbitals are permitted to delocalize over the entire system to minimize the kinetic energy contribution. Yet another density based method is Partition Theory,[35,36] which obtains the total system density by the iterative solution of fragment problems and is thereby able to analyze the movement of charge among those fragments.

In this work, the ALMO-EDA[37] is extended to include spin unrestricted localized molecular orbitals, allowing for application to systems involving open shell species. The ALMO-EDA employs the same fragment blocking of the MO coefficients as the BLW-EDA, solving an efficient implementation[29] of the constrained variational equations for closed shell systems to yield the energy lowering due to polarization. Any SCF treatment of electronic structure can be handled, allowing for mean field HF theory, and most types of density-functional theory (DFT). A new treatment of charge transfer allows separation of forward and back-donation, following the intra-molecular polarization, as well as quantifying the amount of charge transferred in each direction.[38] Subsequently, the closed shell ALMO-EDA has been successfully applied to a growing variety of problems, including neutral water clusters,[39] the hydronium ion,[40] organic reaction mechanisms,[41,42] ligand binding to metal centers,[38] sulfate-water clusters,[43] charge-transfer effects on complex spectra,[44,45] etc.

In the ALMO EDA scheme of Khaliullin *et al.*,[29,37,38] the total interaction energy of a system of fragments is partitioned into contributions from frozen orbital interactions (FRZ), polarization (POL), and charge transfer (CT),

$$\Delta E_{\text{interaction}} = \Delta E_{\text{GEO}} + \Delta E_{\text{FRZ}} + \Delta E_{\text{POL}} + \Delta E_{\text{CT}}. \quad (1)$$

The first term, ΔE_{GEO}, is the energy penalty associated with distorting isolated fragments from their optimal geometries to attain their respective geometries in the interacting complex. The second term, ΔE_{FRZ}, is the energy change associated with bringing infinitely separated, distorted fragments together into the interacting supermolecular geometry without allowing the orbitals, calculated at infinite separation, to relax. Physically, ΔE_{FRZ} includes both electrostatic interactions and Pauli repulsion effects. Electrostatics are favorable when multipole moments on the fragments align properly, but the interaction of overlapping filled orbitals can be quite unfavorable when inter-fragment distances are very short and exclusion requires considerable distortion of the density. The polarization contribution, ΔE_{POL}, is the energy lowering brought about by allowing the frozen orbitals to relax subject to the constraint that they remain absolutely localized (fragment-blocked MO coefficients). This constraint allows for the efficient calculation of a variational polarization energy which precludes the formation of orbitals that span more than one fragment, which is an intuitive picture of the result of charge transfer interactions. The remaining interaction energy, ΔE_{CT}, recovered when the orbitals are allowed to fully relax and delocalize, is thus charge transfer.

The outline of this paper is as follows. The specific equations that are solved for each of the non-trivial components of the interaction energy, Eq. (1), in the case of open shell fragments are summarized in Sec. II. Some computational details are summarized before we turn to a series of pilot examples involving intermolecular interactions of open shell species in Sec. IV. The first class of examples is comparative interactions of methyl radical, methane, tertiary butyl radical, and isobutane with sodium, potassium, hydronium, and ammonium cations. These interactions have been previously examined[46] with NBO methods, and an important role for hydrogen-bonding was elucidated. The second class of examples is relevant to nucleophilic aromatic substitution reactions[47] and involves the benzene radical cation interacting with a series of nucleophiles in both on-top and side-on geometries. The ability of the open shell ALMO-EDA to obtain results that are reasonable and insightful can be assessed from these pilot applications.

II. THEORY

The notation adhered to in this work is as follows: Spatial MO: ψ; Spatial AO: ω; Fragment indices: Capital Roman $X, Y\ldots$; AO indices: lower case Greek $\mu, \nu\ldots$; Virtual MO indices: $a, b\ldots$; Occupied MO indices: $i, j\ldots$; Generic MO indices: $r, s\ldots$. This work incorporates wavefunction representations involving non-orthogonal orbitals and thus makes considerable use of tensors with both covariant (subscript) and contravariant (superscript) indices.[48] Dots are used as placeholders for clear index ordering in quantities that have both covariant and contravariant indices. For instance, the matrix $\mathbf{C}_\alpha$ with matrix elements $(C_\alpha)^{X\mu}_{\bullet\ Yr}$ has rows corresponding to contravariant atomic orbitals and columns corresponding to covariant molecular orbitals. Equations are generally consistent with the covariant integral representation and employ the Einstein summation convention for covariant and contravariant indices with the exception of fragment indices, for which all summations are written explicitly.

A. Frozen energy

The alpha and beta frozen orbitals are absolutely localized, and their MO coefficient matrices, for instance $(C_{\alpha,\text{FRZ}})^{X\mu}_{\bullet\ Xr}$, are obtained as the block diagonal concatenation of fragment blocks of MO coefficient matrices from single point calculations on each fragment in isolation. These calculations are performed at the geometry each fragment adopts within the complex (hitherto referred to as the fragment's complex geometry), rather than the optimal isolated fragment geometry. The AO basis representation of the projector into the subspace spanned by the union of the frozen, occupied subset of MOs, $(T_{\alpha,\text{FRZ}})^{X\mu}_{\bullet\ Xi}$, of these

non-interacting fragments is the "frozen" density matrix, P_{FRZ}:

$$(P_{\alpha,\mathrm{FRZ}})^{X\mu Y\nu} = (T_{\alpha,\mathrm{FRZ}})^{X\mu}_{\bullet\, Xi}(\sigma_\alpha)^{XiYj}\left(T^T_{\alpha,\mathrm{FRZ}}\right)^{\bullet\, Y\nu}_{Yj\,\bullet}. \quad (2)$$

The inclusion of the contravariant alpha occupied MO metric, $(\sigma_\alpha)^{XiYj}$, is necessary to form a valid projector, and thus accounts for Pauli repulsion. It also means the frozen density is not a sum of the non-interacting fragment densities for the general case of non-orthogonal fragment occupied subspaces. The contravariant alpha occupied MO metric is calculated as the inverse of the occupied, occupied block of the covariant alpha MO metric, $(\sigma_\alpha)_{XiYj}$:

$$(\sigma_\alpha)_{XiYj} = \left(T^T_\alpha\right)^{\bullet\, X\mu}_{Xi\,\bullet} S_{X\mu Y\nu}(T_\alpha)^{Y\nu}_{\bullet\, Yj}, \quad (3)$$

$S_{X\mu Y\nu}$ is the covariant atomic orbital overlap metric. The frozen contribution to the interaction energy is simply the difference between the sum of the single point energies for each isolated fragment in its complex geometry and the trace of the frozen density with the full complex's core Hamiltonian, $\mathbf{H}_{\mathrm{core}}$, and Fock matrices, $\mathbf{F}_\alpha$ and $\mathbf{F}_\beta$, formed using the same frozen density:

$$\begin{aligned}\Delta E_{\mathrm{FRZ}} = \frac{1}{2}\mathrm{Tr}[&\mathbf{P}_{\alpha,\mathrm{FRZ}}(\mathbf{H}_{\mathrm{core}} + \mathbf{F}_\alpha[\mathbf{P}_{\alpha,\mathrm{FRZ}}, \mathbf{P}_{\beta,\mathrm{FRZ}}]) \\ &+ \mathbf{P}_{\beta,\mathrm{FRZ}}(\mathbf{H}_{\mathrm{core}} + \mathbf{F}_\beta[\mathbf{P}_{\alpha,\mathrm{FRZ}}, \mathbf{P}_{\beta,\mathrm{FRZ}}])] \\ &- \sum_Z^{\mathrm{Frgm}} E_{Z,\mathrm{Complex}}. \end{aligned} \quad (4)$$

B. Polarization

The unrestricted ALMO wavefunction is the usual single Slater determinant of occupied spin molecular orbitals but with the constraint: the MO coefficient matrix must be block-diagonal in the fragments comprising the complex. This constraint is placed on the AO expansions of covariant spatial MO's for each spin:

$$|\psi_{Xr}\rangle_\alpha = |\omega_{X\mu}\rangle(C_\alpha)^{X\mu}_{\bullet\, Xr}. \quad (5)$$

The frozen wavefunction is itself an ALMO wavefunction by construction, and is an appropriate initial guess for the ALMO SCF. The ALMO SCF is the variational energy lowering resulting from the relaxation of the frozen orbitals within this constraint of absolute locality that defines the polarization contribution in the ALMO EDA scheme. The block diagonal expansion of MOs inherently leads to non-orthogonal molecular orbitals between fragments for non-orthogonal AO basis sets because there are not in general a sufficient number of degrees of freedom in the non-zero blocks to achieve orthogonality.[49]

With the ALMO constraint defined, the remaining portions of this section are thus devoted to a collection and recapitulation of the derivations of: the Hartree-Fock-like equations of Gianinetti[50,51] and Stoll[49] which use the same AO expansion and make no assumption of orthogonality, the corresponding Direct Inversion of the Iterative Subspace (DIIS) error vector equation,[29] and the expressions used in charge transfer analysis.[38] The equations are presented assuming spin unrestricted spatial orbitals.

1. Unrestricted Gianinetti and Stoll equations

The energy for a single Slater determinant with unrestricted spatial orbitals and its derivative with respect to a change in alpha occupied orbital coefficients are:

$$E = \frac{1}{2}\mathrm{Tr}[\mathbf{P}_\alpha(\mathbf{H}_{\mathrm{core}} + \mathbf{F}_\alpha) + \mathbf{P}_\beta(\mathbf{H}_{\mathrm{core}} + \mathbf{F}_\beta)], \quad (6)$$

$$\begin{aligned}\frac{\partial E}{\partial (T_\alpha)^{X\gamma}_{\bullet\, Xi}} &= \sum_{YZ}^{\mathrm{Frgm}} \frac{\partial E}{\partial (P_\alpha)^{Z\lambda,Y\sigma}} \frac{\partial (P_\alpha)^{Z\lambda,Y\sigma}}{\partial (T_\alpha)^{X\gamma}_{\bullet\, Xi}} \\ &= \sum_{YZ}^{\mathrm{Frgm}} (F_\alpha)_{Y\sigma,Z\lambda} \frac{\partial (P_\alpha)^{Z\lambda,Y\sigma}}{\partial (T_\alpha)^{X\gamma}_{\bullet\, Xi}}. \end{aligned} \quad (7)$$

The required partial derivatives are:

$$\begin{aligned}\frac{\partial (P_\alpha)^{Z\lambda,Y\sigma}}{\partial (T_\alpha)^{X\gamma}_{\bullet\, Xi}} &= \delta^{Z\lambda}_{X\gamma}(\sigma_\alpha)^{Xi,Yj}(T^T_\alpha)^{\bullet\, Y\sigma}_{Yj\,\bullet} \\ &+ (T_\alpha)^{Z\lambda}_{\bullet\, Zk}\left(\frac{\partial (\sigma_\alpha)^{Zk,Yj}}{\partial (T_\alpha)^{X\gamma}_{\bullet\, Xi}}\right)(T^T_\alpha)^{\bullet\, Y\sigma}_{Yj\,\bullet} \\ &+ (T_\alpha)^{Z\lambda}_{\bullet\, Zk}(\sigma_\alpha)^{Zk,Xi}\delta^{Y\sigma}_{X\gamma}, \end{aligned} \quad (8)$$

$$\begin{aligned}\frac{\partial (\sigma_\alpha)^{Zk,Yj}}{\partial (T_\alpha)^{X\gamma}_{\bullet\, Xi}} &= -\sum_{AB}^{\mathrm{Frgm}} (\sigma_\alpha)^{Zk,Al}\left(\frac{\partial (\sigma_\alpha)_{Al,Bm}}{\partial (T_\alpha)^{X\gamma}_{\bullet\, Xi}}\right)(\sigma_\alpha)^{Bm,Yj} \\ &= -\sum_{A}^{\mathrm{Frgm}} \Big((\sigma_\alpha)^{Zk,Al}(T^T_\alpha)^{\bullet\, A\mu}_{Al\,\bullet} S_{A\mu,X\gamma}(\sigma_\alpha)^{Xi,Yj} \\ &+ (\sigma_\alpha)^{Zk,Xi} S_{X\gamma,A\mu}(T_\alpha)^{A\mu}_{\bullet\, Al}(\sigma_\alpha)^{Al,Yj}\Big). \end{aligned} \quad (9)$$

After making the requisite substitutions, one obtains:

$$\begin{aligned}\frac{\partial E}{\partial (T_\alpha)^{X\gamma}_{\bullet\, Xi}} = 2\sum_{YZ}^{\mathrm{Frgm}} \Bigg[&\left(\delta^{Z\lambda}_{X\gamma} - \sum_A^{\mathrm{Frgm}} S_{X\gamma,A\mu}(P_\alpha)^{A\mu,Z\lambda}\right) \\ &\times (F_\alpha)_{Z\lambda,Y\sigma}(T_\alpha)^{Y\sigma}_{\bullet\, Yj}(\sigma_\alpha)^{Yj,Xi}\Bigg]. \end{aligned} \quad (10)$$

From the above equation, we obtain the following matrix equation for stationarity for each fragment, X, and each spin:

$$\mathbf{0} = \left[(\mathbf{1} - \mathbf{S}\mathbf{P}_\alpha)\mathbf{F}_\alpha\mathbf{T}_\alpha\boldsymbol{\sigma}_\alpha^{-1}\right]_{XX}, \quad (11)$$

$\mathbf{T}_\alpha$ is again defined as the occupied block of $\mathbf{C}_\alpha$. Equation (11) represents the usual requirement that the occupied-virtual block of the Fock matrix should be zero at convergence, while taking into account the reduced flexibility in the ALMO expansion. Occupied-occupied mixings do not alter the energy, and on-fragment rotations do not

violate the constraint of the ALMO expansion. Thus, one is free to select the fragment diagonal blocks of the occupied-occupied contravariant-contravariant MO Fock matrix as diagonal without loss of generality,

$$[\boldsymbol{\sigma}_\alpha^{-1}\mathbf{T}_\alpha^T\mathbf{F}_\alpha\mathbf{T}_\alpha\boldsymbol{\sigma}_\alpha^{-1} - \epsilon_\alpha]_{XX} = 0. \tag{12}$$

There is a more amenable form of the above eigenvalue problem which can be solved for the covariant MOs on each fragment. It can be obtained by applying the following fragment-specific substitution:

$$\begin{aligned}
&(T_\alpha)^{Z\nu}_{\bullet\ Zl}(\sigma_\alpha)^{Zl,Xi} \\
&\quad= \sum_Y^{\text{Frgm}}\sum_j (T_\alpha)^{Z\nu}_{\bullet\ Zl}(\sigma_\alpha)^{Zl,Xj}(\sigma_\alpha)^{Xj,Yk}(\sigma_\alpha)_{YkXi} \\
&\quad= \sum_Y^{\text{Frgm}}\sum_j \left((T_\alpha)^{Z\nu}_{\bullet\ Zl}(\sigma_\alpha)^{Zl,Xj}(\sigma_\alpha)^{Xj,Yk}(T_\alpha^T)^{\bullet\ Y\mu}_{Yk\ \bullet}\right) \\
&\qquad\times S_{Y\mu,X\lambda}(T_\alpha)^{X\lambda}_{\bullet\ Xi} \\
&\quad= \sum_Y^{\text{Frgm}}\left(P^X_{\alpha,G}\right)^{Z\nu,Y\mu}S_{Y\mu,X\lambda}(T_\alpha)^{X\lambda}_{\bullet\ Xi}.
\end{aligned} \tag{13}$$

With the following definition for the quantity $(P^X_{\alpha,G})^{Z\nu,Y\mu}$, which appears in the equations of Gianinetti:

$$(P^X_{\alpha,G})^{Z\nu,Y\mu} = \sum_j (T_\alpha)^{Z\nu}_{\bullet\ Zl}(\sigma_\alpha)^{Zl,Xj}(\sigma_\alpha)^{Xj,Yk}\left(T_\alpha^T\right)^{\bullet\ Y\mu}_{Yk\ \bullet}.$$

The contraction over mismatched Xj indices above is valid because it corresponds to multiplication by the identity:

$$\left[\sigma_\alpha^{-1}\sigma_\alpha\right]_{XX} = \mathbf{I}_{XX}. \tag{14}$$

Together with Eqs. (11) and (12) this substitution yields the eigenvalue equations of Gianinetti for each fragment and spin:

$$\begin{aligned}
&\left[\left(\mathbf{1} - \mathbf{SP}_\alpha + \mathbf{SP}^X_{\alpha,G}\right)\mathbf{F}_\alpha\left(\mathbf{1} - \mathbf{P}_\alpha\mathbf{S} + \mathbf{P}^X_{\alpha,G}\mathbf{S}\right)\right]_{XX}[\mathbf{C}_\alpha]_{XX} \\
&\quad= \left[\left(\mathbf{S} - \mathbf{SP}_\alpha\mathbf{S} + \mathbf{SP}^X_{\alpha,G}\mathbf{S}\right)\right]_{XX}[\mathbf{C}_\alpha]_{XX}[\epsilon_\alpha]_{XX}.
\end{aligned} \tag{15}$$

The additional projector into the orthogonal complement of the occupied space, $(\mathbf{S} - \mathbf{SP}_\alpha\mathbf{S}) \equiv \mathbf{SQ}_\alpha\mathbf{S}$, in the effective overlap of the generalized eigenvalue problem is necessary to avoid singularities. Alternatively, using the following substitution involving the quantity $(P^X_{\alpha,S})^{Z\nu,X\mu}$ found in Stoll's equations:

$$\begin{aligned}
(T_\alpha)^{Z\nu}_{\bullet\ Zl}(\sigma_\alpha)^{Zl,Xi} &= (T_\alpha)^{Z\nu}_{\bullet\ Zl}(\sigma_\alpha)^{Zl,Xj}\left(T_\alpha^T\right)^{\bullet\ X\mu}_{Xj\ \bullet}S_{X\mu,X\lambda}(T_\alpha)^{X\lambda}_{\bullet\ Xi} \\
&= \left(P^X_{\alpha,S}\right)^{Z\nu,X\mu}S_{X\mu,X\lambda}(T_\alpha)^{X\lambda}_{\bullet\ Xi}, \\
\left(P^X_{\alpha,S}\right)^{Z\nu,X\mu} &= (T_\alpha)^{Z\nu}_{\bullet\ Zl}(\sigma_\alpha)^{Zl,Xj}\left(T_\alpha^T\right)^{\bullet\ X\mu}_{Xj\ \bullet},
\end{aligned} \tag{16}$$

with Eqs. (11) and (12) yields the fragment-by-fragment and spin-by-spin eigenvalue equations of Stoll:

$$\begin{aligned}
&\left[\left(\mathbf{1} - \mathbf{SP}_\alpha + \mathbf{SP}^X_{\alpha,S}\right)\mathbf{F}_\alpha\left(\mathbf{1} - \mathbf{P}_\alpha\mathbf{S} + \mathbf{P}^X_{\alpha,S}\mathbf{S}\right)\right]_{XX}[\mathbf{C}_\alpha]_{XX} \\
&\quad= [\mathbf{S}]_{XX}[\mathbf{C}_\alpha]_{XX}[\epsilon_\alpha]_{XX}.
\end{aligned} \tag{17}$$

In both Eqs. (15) and (17), the problem of obtaining the polarized ALMO wavefunction of the supermolecular system is reduced to iterative fragment-by-fragment eigenvalue problems for each spin, coupled through the density and Fock builds. These equations arise from the minimization of the energy given the constraint of absolute locality in the MOs and do not involve any deletion of Fock matrix elements. Indeed, the full AO basis Fock matrix is involved. Additionally, only the contravariant metric for the occupied subspace is required, eliminating the need for the inversion of the full MO metric. Indeed the effort necessary to solve these equations iteratively is significantly less than required for conventional full diagonalization, as has previously been demonstrated in the closed shell case.[29]

2. Unrestricted DIIS error vector

The DIIS algorithm[52] can be used to accelerate the convergence of the above equations with a small modification of the error vector that accounts for the reduction in degrees of freedom associated with the constrained AO expansion. The DIIS error vector is derived by considering an infinitesimal orthogonal update to the alpha density matrix correct to first order in the block diagonal anti-symmetric matrix, Δ_α, parametrizing the update:

$$\begin{aligned}
(\tilde{P}_\alpha)^{K\kappa,L\lambda} \approx\ &(T_\alpha)^{K\kappa}_{\bullet\ Kk}(\tilde{\sigma}_\alpha)^{Kk,Ll}\left(T_\alpha^T\right)^{\bullet\ L\lambda}_{Ll\ \bullet} \\
&+ (T_\alpha)^{K\kappa}_{\bullet\ Kk}\sigma_\alpha^{Kk,Ll}\left(T_\alpha^T\right)^{\bullet\ L\rho}_{Ll\ \bullet}S_{L\rho,L\pi}(\Delta_\alpha)^{L\pi,L\lambda} \\
&- (\Delta_\alpha)^{K\kappa,K\gamma}S_{K\gamma,K\mu}(T_\alpha)^{K\mu}_{\bullet\ Kk}\sigma_\alpha^{Kk,Ll}(T_\alpha^T)^{\bullet\ L\lambda}_{Ll\ \bullet}.
\end{aligned} \tag{18}$$

Here $(\tilde{P})^{K\kappa,L\lambda}_\alpha$ is the updated density and $(\tilde{\sigma})^{KkLl}_\alpha$ is the inverse of the metric of updated occupied MOs correct through first order in Δ_α:

$$\begin{aligned}
(\tilde{\sigma}_\alpha)_{Mm,Nn} \approx\ &\left(T_\alpha^T\right)^{\bullet\ M\mu}_{Mm\ \bullet}S_{M\mu,N\nu}(T_\alpha)^{N\nu}_{\bullet\ Nn} \\
&+ \left(T_\alpha^T\right)^{\bullet\ M\xi}_{Mm\ \bullet}S_{M\xi,M\gamma}(\Delta_\alpha)^{M\gamma,M\mu}S_{M\mu,N\nu}(T_\alpha)^{N\nu}_{\bullet\ Nn} \\
&- \left(T_\alpha^T\right)^{\bullet\ M\mu}_{Mm\ \bullet}S_{M\mu,N\nu}(\Delta_\alpha)^{N\nu,N\rho}S_{N\rho,N\pi}(T_\alpha)^{N\pi}_{\bullet\ Nn}.
\end{aligned} \tag{19}$$

This transformation thus preserves MO overlap through first order on a fragment but allows inter-fragment overlaps to change, as desired. The error vector is then the derivative of the energy with respect to this update evaluated at $\Delta_\alpha = 0$:

$$\begin{aligned}
\frac{\partial E}{\partial(\Delta_\alpha)^{X\xi,X\tau}} &= \sum_{KL}^{\text{Frgm}}\frac{\partial E}{\partial(\tilde{P}_\alpha)^{K\kappa,L\lambda}}\frac{\partial(\tilde{P}_\alpha)^{K\kappa,L\lambda}}{\partial(\Delta_\alpha)^{X\xi,X\tau}} \\
&= \sum_{KL}^{\text{Frgm}}(F_\alpha)_{L\lambda,K\kappa}\frac{\partial(\tilde{P}_\alpha)^{K\kappa,L\lambda}}{\partial(\Delta_\alpha)^{X\xi,X\tau}}.
\end{aligned} \tag{20}$$

The additional derivatives needed are:

$$\frac{\partial(\tilde{P}_\alpha)^{K\kappa,L\lambda}}{\partial(\Delta_\alpha)^{X\xi,X\tau}} = (T_\alpha)^{K\kappa}_{\bullet\,Kk}\frac{\partial(\tilde{\sigma}_\alpha)^{Kk,Ll}}{\partial(\Delta_\alpha)^{X\xi,X\tau}}(T_\alpha^T)^{\bullet\,L\lambda}_{Ll\,\bullet} - \delta^{K\kappa}_{X\xi}\delta^{K\phi}_{X\tau}S_{K\phi K\eta}(T_\alpha)^{K\eta}_{\bullet\,Kk}(\sigma_\alpha)^{Kk,Ll}\left(T_\alpha^T\right)^{\bullet\,L\lambda}_{Ll\,\bullet} + (T_\alpha)^{K\kappa}_{\bullet\,Kk}(\sigma_\alpha)^{Kk,Ll}\left(T_\alpha^T\right)^{\bullet\,L\gamma}_{Ll\,\bullet}S_{L\gamma L\epsilon}\delta^{L\epsilon}_{X\xi}\delta^{L\lambda}_{X\tau}, \tag{21}$$

$$\frac{\partial(\tilde{\sigma}_\alpha)^{Kk,Ll}}{\partial(\Delta_\alpha)^{X\xi,X\tau}} = \sum_M^{\text{Frgm}}(\sigma_\alpha)^{Kk,Mm}\left(T_\alpha^T\right)^{\bullet\,M\mu}_{Mm\,\bullet}S_{M\mu,X\xi}S_{X\tau,X\rho}(T_\alpha)^{X\rho}_{\bullet\,Xn}(\sigma_\alpha)^{Xn,Ll} - \sum_N^{\text{Frgm}}(\sigma_\alpha)^{Kk,Xm}\left(T_\alpha^T\right)^{\bullet\,X\lambda}_{Xm\,\bullet}S_{X\lambda,X\xi}S_{X\tau,N\nu}(T_\alpha)^{N\nu}_{\bullet\,Nn}(\sigma_\alpha)^{Nn,Ll}. \tag{22}$$

The DIIS error vector for the convergence of the Gianinetti and Stoll equations is thus:

$$[\mathbf{R}_\alpha]_{XX} = \mathbf{S}_{XX}\left[\mathbf{P}_\alpha\mathbf{F}_\alpha(\mathbf{P}_\alpha\mathbf{S}-\mathbf{1})\right]_{XX} - \left[(\mathbf{S}\mathbf{P}_\alpha-\mathbf{1})\mathbf{F}_\alpha\mathbf{P}_\alpha\right]_{XX}\mathbf{S}_{XX}, \tag{23}$$

which resembles the error vector equation of Pulay[52] but, like the equations to be solved, is both fragment-by-fragment and spin-by-spin.

C. Charge transfer

As mentioned previously, the construction of the polarized wavefunction is such that it prevents the interfragment orbital mixings intuitively associated with charge transfer. An energy lowering from charge transfer interactions can thus be calculated as the difference between the energy of the unconstrained full SCF solution and the energy of the polarized solution. This is termed the variational charge transfer contribution to the energy, V-CT. Moreover, the ALMO wavefunction strictly precludes any movement of charge population between fragments by the Mulliken definition, forcing all such charge rearrangements to occur during the charge transfer phase of the calculation; the only time that the constraint of absolute locality is not enforced. It is thus possible to evaluate net movement of charge between fragments during charge transfer by Mulliken population analysis of the full SCF density.

It is often helpful to think about charge transfer interactions in terms of forward and back donation of electrons through specific orbital interactions. A textbook example is forward and back-donation in the bonding of ligands such as CO to a transition metal center.[38] Such directional, orbital specific information can be obtained by exploiting the stationarity of the variational, polarized ALMO wavefunction, Eq. (11), specifically that the polarized Fock matrix elements between covariant virtual orbitals projected into the orthogonal complement of the occupied subspace, **Q**, and contravariant occupied orbitals on the same fragment are zero. The projected virtuals, $\tilde{\mathbf{V}}$, used in the analysis of charge transfer are defined in terms of the unprojected, fragment blocked virtuals, **V**, obtained from converging the Gianinetti or Stoll equations as

$$\tilde{\mathbf{V}}_\alpha = \mathbf{Q}_\alpha\mathbf{S}\mathbf{V}_\alpha = (\mathbf{I}-\mathbf{P}_\alpha\mathbf{S})\mathbf{V}_\alpha,$$
$$(\tilde{V}_\alpha)^{Z\mu}_{\bullet\,X\tilde{a}} = \left[\delta^{Z\mu}_{X\nu} - \sum_Y^{\text{Frgm}}(P_\alpha)^{Z\mu,Y\lambda}S_{Y\lambda,X\nu}\right](V_\alpha)^{X\nu}_{\bullet\,Xa}, \tag{24}$$

where the index $X\tilde{a}$ denotes the projected counterpart of virtual orbital a on fragment X. These virtual orbitals are in general not absolutely localized, but still carry a fragment label, and are still quite well localized.

The infinite-order singles perturbation theory (Roothaan step) energy lowering associated with the relaxation of the ALMO constraint must also be necessarily charge transfer in character, and is given by Refs. 38 and 53

$$E_{\alpha,\text{P-CT}} = \text{Tr}\left[\mathbf{P}_\alpha\mathbf{F}_\alpha\mathbf{Q}_\alpha\mathbf{X}_\alpha\right] = \sum_{WXYZ}^{\text{Frgm}}(\sigma_\alpha)^{Xi,Zk}(T_\alpha^T)^{\bullet\,Z\mu}_{Zk\,\bullet}(F_\alpha)_{Z\mu,W\nu}(\tilde{V}_\alpha)^{W\nu}_{\bullet\,Y\tilde{a}}(X_\alpha)^{Y\tilde{a}}_{\bullet\,Xi} = \sum_{X\neq Y}^{\text{Frgm}}(F_\alpha)^{Xi}_{\bullet\,Y\tilde{a}}(X_\alpha)^{Y\tilde{a}}_{\bullet\,Xi}, \tag{25}$$

The matrix of mixing parameters, $(X_\alpha)^{Y\tilde{a}}_{\bullet\,Xi}$, is determined by iteratively solving:

$$(F_\alpha)^{Y\tilde{a}}_{\bullet\,Xi} + \sum_Z^{\text{Frgm}}(F_\alpha)^{Y\tilde{a}}_{\bullet\,Z\tilde{b}}(X_\alpha)^{Z\tilde{b}}_{\bullet\,Xi} - \sum_W^{\text{Frgm}}(X_\alpha)^{Y\tilde{a}}_{\bullet\,Wj}(F_\alpha)^{Wj}_{\bullet\,Xi} - \sum_{WZ}^{\text{Frgm}}(X_\alpha)^{Y\tilde{a}}_{\bullet\,Wj}(F_\alpha)^{Wj}_{\bullet\,Z\tilde{b}}(X_\alpha)^{Z\tilde{b}}_{\bullet\,Xi} = 0. \tag{26}$$

This matrix of parameters in general has non-zero values describing rotations of all occupied orbitals on each fragment into all virtual orbitals on all fragments. However, because of the stationarity of the constrained solution, only amplitudes corresponding to inter-fragment orbital mixings give non-zero contributions to the Roothaan step energy correction, Eq. (25).

In the case of supermolecular systems composed of only two fragments, X and Y, transformation of fragment X's occupied orbitals by the right eigenvectors, $(R_\alpha)^{\bullet\,X\bar{j}}_{Xi\,\bullet}$, and fragment Y's projected virtual orbitals by the left eigenvectors, $(L_\alpha)^{Y\tilde{a}}_{\bullet\,Y\bar{b}}$, from the Singular Value Decomposition (SVD) of $(X_\alpha)^{Y\tilde{a}}_{\bullet\,Xi}$ provides a basis, $\bar{r}$, in which each occupied orbital on X mixes with exactly one virtual orbital on Y because of the diagonal structure of $\mathbf{X}_\alpha$ in the SVD basis, $(x_\alpha)^{Y\bar{b}}_{\bullet\,X\bar{j}}$. In the ALMO EDA, these orbitals that allow for the description of charge transfer in terms of pairwise orbital interactions with corresponding energy lowering (cf. Eq. (28)) are termed

complementary occupied-virtual orbital pairs (COVPs),

$$(X_\alpha)^{Y\tilde{a}\bullet}_{\bullet Xi} = (L_\alpha)^{Y\tilde{a}\bullet}_{\bullet Y\tilde{b}}(x_\alpha)^{Y\tilde{b}\bullet}_{\bullet X\tilde{j}}(R^T_\alpha)^{X\tilde{j}\bullet}_{\bullet Xi}, \tag{27}$$

$$E^{X\to Y}_{\alpha,\text{P-CT}} = (R^T_\alpha)^{X\tilde{j}\bullet}_{\bullet Xi}(F_\alpha)^{Xi\bullet}_{\bullet Y\tilde{a}}(L_\alpha)^{Y\tilde{a}\bullet}_{\bullet Y\tilde{b}}(x_\alpha)^{Y\tilde{b}\bullet}_{\bullet X\tilde{j}}. \tag{28}$$

A similar scheme can be used to ascribe a portion of the charge transferred to each orbital pair interaction

$$Q^{X\to Y}_{\alpha,\text{P-CT}} = (R^T_\alpha)^{X\tilde{j}\bullet}_{\bullet Xi}(P'_\alpha)^{Xi\bullet}_{\bullet Y\tilde{a}}(L_\alpha)^{Y\tilde{a}\bullet}_{\bullet Y\tilde{b}}(x_\alpha)^{Y\tilde{b}\bullet}_{\bullet X\tilde{j}}, \tag{29}$$

where $\mathbf{P}'_\alpha$ is the updated density matrix after the Roothaan step. Furthermore, because one can perform the same procedure for the matrix $(X_\alpha)^{X\tilde{a}\bullet}_{\bullet Yi}$, it is possible to decompose charge flow (and energy lowering) into contributions from forward and back-donation rather than the simple description of net charge flow afforded by traditional population analysis. This procedure can be conducted separately in the alpha and beta spaces, sometimes revealing interesting asymmetry (and sometimes intriguing lack of asymmetry) in the charge transfer components for the two spins in open shell systems.

While charge transfer analysis and, in the case of two fragment systems, COVP analysis can provide very insightful ways of looking at interactions between fragments, both depend on perturbation theory, a single matrix, $\mathbf{X}$, parametrizing the orbital mixings away from the polarized solution to obtain fragment-to-fragment and orbital-to-orbital descriptions, respectively. The use of perturbation theory means that some of the interaction energy is missing. The difference between the variational and perturbative charge transfer energy lowerings is termed the higher order charge transfer contribution, E_{HO}, as it necessarily involves orbital rotations corresponding to both intrafragment repolarization and further interfragment charge transfer occurring in response to the initial, pairwise decomposable charge transfer,

$$E_{\text{V-CT}} = E_{\text{P-CT}} + E_{\text{HO}}. \tag{30}$$

The energy lowering associated with higher order orbital relaxations is minimal for weakly interacting system where a perturbative treatment of dative interactions is valid. In this work, the higher order correction constitutes only a small fraction of the variational charge transfer interaction, and so variational charge transfer energies are used predominantly for simplicity (recovering the full binding energy in fewer terms) while perturbative charge transfer energies are used as needed in the discussion of COVP analysis results. It should be noted that, by construction, basis set superposition error (BSSE) does not enter into the frozen or polarized terms; however, the charge transfer term does contain energy lowering attributable to BSSE effects and can be corrected if desired.

To conclude, it is worthwhile to note that the variational approach to defining the polarization contribution is a greedy one. All energy lowering associated with the molecule-blocked form of the ALMO constraint is associated with polarization. This contribution will implicitly include any part of charge transfer that can be described by the intersection of the one-particle Hilbert spaces associated with interacting molecules. Thus the values of polarization may include a contaminating component from charge transfer, while CT itself may be underestimated. However, we shall see from the results that the separation appears to be well-defined with the reasonably large Pople basis (6-311++G(3df,3pd)) employed in this study. For closed shell systems, even larger basis sets have been successfully used in applications such as the water dimer.[29,39] Nonetheless, as we demonstrate elsewhere,[54] the values of polarization and charge transfer do not have well-defined complete basis set limits, but in fact are metastable in standard sequences of basis sets. The interested reader is invited to look at results in the supplementary materials[55] for the 6-31+G(d,p) basis, considerably smaller than that employed in the remainder of this work, to assess the qualitative significance of the different energy partitionings between polarization and charge transfer. The larger 6-311++G(3df,3pd) basis is chosen to better represent the total interaction between fragments. It should also be noted that the ALMO EDA at the SCF level does not separate out a contribution from dispersion as the construction of some density functionals might suggest is possible. Indeed, the interaction energy from pairwise potentials in -D methods[56] appears in the frozen term as it is unaltered as the density relaxes; however, this would not be the behavior of dispersion interactions in the exact density functional, which would incorporate some contribution from dispersion at each stage of the density relaxation. Thus, in order that the ALMO EDA maintain the correct behavior for the exact functional and in order that it also not be wedded to a specific density functional form, a dispersion term is not defined at the SCF level in the ALMO EDA.

III. COMPUTATIONAL DETAILS

A development version of Q-Chem 3.2[57] was used for all calculations. Geometries for each system discussed in this work were calculated at the B3LYP/6-311++G(3df,3pd) level and verified to be valid minima by frequency calculations at the same level of theory.[55] ALMO EDA with single Roothaan step and subsequent exact SCF CT correction as well as COVP analysis calculations were performed on each system at the B3LYP[58]/6-311++G(3df,3pd) level. Radical fragments in this work were chosen to be doublets with unpaired electrons of spin alpha. In the interest of completeness, ALMO EDA calculations were also performed on the same B3LYP/6-311++G(3df,3pd) system geometries using the 6-31+G(d,p) basis set and with the functionals: ωB97,[59] ωB97X,[59] ωB97x-D,[60] M06,[61] and M06-2X.[61] The results for a subset of the systems considered appear in the supplementary materials,[55] and because they do not give a qualitatively different interpretation of the interactions, only the B3LYP/6-311++G(3df,3pd) EDA results will be discussed in the remainder of this work. Geometric distortions in all cases were determined using B3LYP/6-311++G(3df,3pd) isolated fragment geometries. Where applicable results were counterpoise corrected in order to account for spurious Basis Set Superposition Error. Orbital plots were generated using the Chimera[62] visualization program.

IV. APPLICATIONS

A. Alkyl radicals

Intermolecular complexes involving alkyl radicals such as $CH_3^\bullet$ and $(CH_3)_3C^\bullet$ interacting with cations are interesting model systems for understanding the stabilization of transition structures associated with bond making and breaking reactions in proteins when OH and NH groups are present.[46,63] Additionally, closed shell analogs can be easily constructed to compare the inter-fragment interactions. The cation pairs H_3O^+/Na^+ and NH_4+/K^+ are of comparable size and have the same charge, suggesting that each member of the pair should be able to achieve comparable electrostatic interactions because the monopoles will be at similar intermolecular distances. However, the alkali metal cations have only negligible orbital interactions (CT) with the alkyl species.[46] After recognizing the shortcomings of NBO/NEDA methods for analyzing the strong interactions in such systems, Hammerum[46] identified the differences in the binding energies of the molecular/alkali cation pairs as arising from hydrogen bonding interactions, noting that binding energies for the members of each cation pair with closed shell alkyl species were comparable.

Table I shows the partitioning of the total interaction energy according the ALMO EDA, and a graphical version of the data is presented in Fig. 1.

From both of these presentations, it is apparent that charge transfer orbital interactions are of negligible importance for systems containing alkali cations, as chemical intuition would suggest. Conversely, the hydronium and ammonium systems show considerable charge transfer interaction even with the closed shell alkyl species. The difference in CT between alkali and molecular cation pairs is however considerably greater than the difference in binding energy. The closer contacts in the molecular cation systems that are necessary to achieve optimal orbital overlap also incur large penalties to binding in the GD and FRZ terms, which are only partially canceled by the increased CT and polarization brought about by the closer (stronger) interaction.

TABLE I. Alkyl Radical ALMO EDA Results: EDA terms (kJ/mol) for systems containing an alkane or alkyl radical and a cation, either alkali or molecular. Note that the pairs H_3O^+/Na^+ and NH_4^+/K^+ are of comparable size, so one should expect comparable electrostatic interactions; however, FRZ and POL terms are noticeably larger in magnitude for the systems with molecular cations due to the closer interaction brought about by the charge transfer interactions exclusive to the molecular systems.

Alkyl species	Cation	GD	FRZ	POL	V-CT	Bind
$(CH_3)_3C^\bullet$	K^+	1.4	−9.6	−31.0	−2.4	−41.6
	NH_4^+	9.9	22.8	−54.8	−42.7	−64.9
	Na^+	2.3	−19.7	−52.8	−0.7	−71.0
	H_3O^+	82.1	83.3	−159.0	−130.6	−124.2
$(CH_3)_3CH$	K^+	2.0	10.8	−32.5	−1.5	−21.2
	NH_4^+	2.3	18.7	−33.8	−12.0	−24.7
	Na^+	4.3	12.2	−60.5	−1.1	−45.0
	H_3O^+	11.9	48.0	−72.3	−39.4	−51.8
$CH_3^\bullet$	K^+	1.6	−10.3	−14.5	−1.3	−24.5
	NH_4^+	3.8	6.1	−24.0	−23.2	−37.3
	Na^+	1.8	−16.2	−27.9	−1.5	−43.7
	H_3O^+	14.3	27.7	−53.2	−58.2	−69.4
CH_4	K^+	1.0	0.6	−15.5	−0.9	−14.7
	NH_4^+	1.5	8.0	−20.2	−8.1	−18.7
	Na^+	2.2	−0.7	−31.1	−1.0	−30.6
	H_3O^+	6.2	24.6	−44.0	−25.6	−38.8

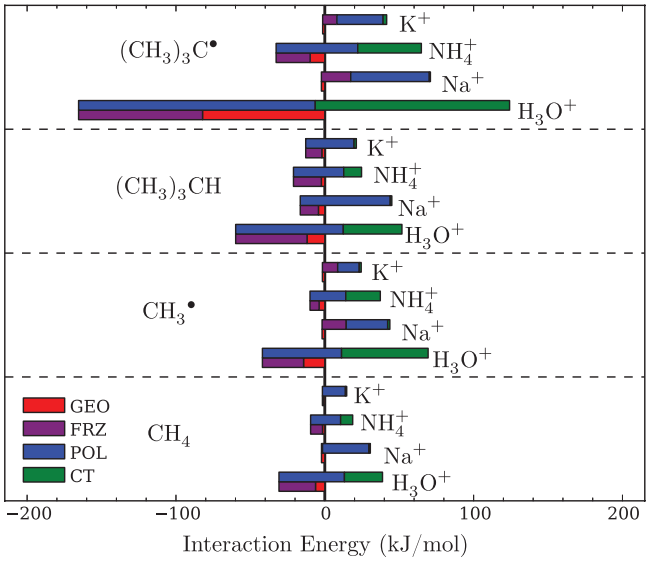

FIG. 1. Alkyl Radical ALMO EDA Results: Unfavorable terms, such as geometric distortion are placed on the bottom of a double bar and grow to the left (negative). On the top bar, favorable terms such as polarization grow to the right (positive). By construction, the binding energy can then be read as the length of the bar to the right. Charge transfer is of much greater importance in systems involving molecular cations and, among those, for systems including a radical.

The inter-fragment orbital gap (the energy difference between the donor HOMO and the acceptor LUMO) was calculated as the difference between the experimental ionization potential of the alkyl species less the experimental ionization potential of D_3O or NH_4.[64] A plot of charge transfer energy lowering versus the inverse of the inter-fragment gap for systems containing a molecular cation, H_3O^+ or NH_4^+, appears in Fig. 2. This plot shows a rapidly increasing charge transfer

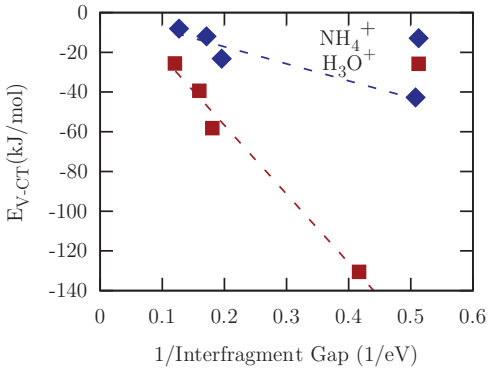

FIG. 2. Variational Charge Transfer ($E_{V\text{-}CT}$; kJ/mol) Plotted Against the Inverse of the Interfragment Orbital Energy Gap (eV; ionization potential of alkyl species less the electron affinity of the cation): Data are for alkyl systems containing molecular cations. The proportionality of energy denominators to energy lowerings shown by the linear relationships echoes the physicality of traditional perturbative treatments of orbital interactions. Groupings are motivated by steric considerations, and the relative slopes can be explained by the greater proton affinity of ammonia.

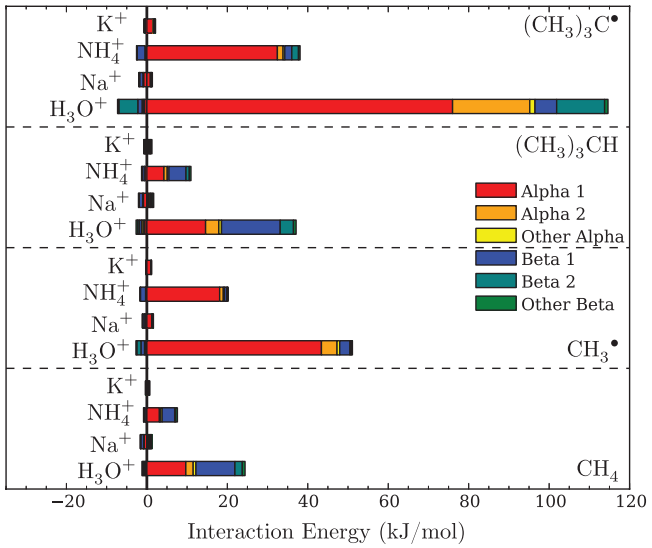

FIG. 3. Alkyl COVP Results: All interactions are favorable, and the direction of growth from the zero line indicates the directionality of the charge transfer. Energy contributions to the left of zero involve COVPs with the acceptor orbital on the alkyl species while those on the right correspond to charge donation to the cation. Contributions from orbital interactions in the alpha space are denoted with warm colors and those in the beta space with cool colors to facilitate the recognition of symmetry or asymmetry with respect to spin. Each color indicates a different occupied-virtual orbital pair's energy contribution. Additionally, the total length of the bar indicates the magnitude of the charge transfer energy lowering calculated by perturbation theory. Notice that, in the alkali cation cases, donation is negligible while, for systems containing H_3O^+ and NH_4^+, charge transfer is primarily to the cation, symmetric with respect to spin for closed shell cases and primarily from the higher energy alpha HOMO of the alkyl species for the open shell cases.

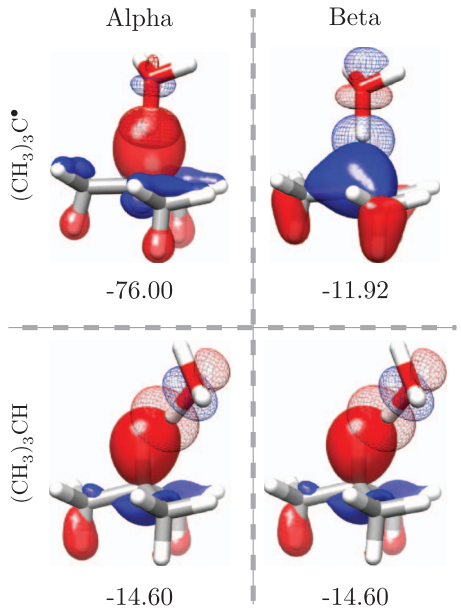

FIG. 4. Representative COVP Images for Alkyl Systems: The most important COVPs in the alpha and beta spaces for the interaction of hydronium with the t-butyl radical ($(CH_3)_3C^\bullet$) and its closed shell analog ($(CH_3)_3CH$). The charge transfer energy lowering (kJ/mol) associated with each orbital pair is also shown. The virtual (acceptor) orbital of the pair is depicted as a mesh isosurface while that for the occupied (donor) orbital is represented with a translucent isosurface. The charge transfer interaction with the radical is reminiscent of chemical bonding with the alpha space charge transfer occurring from a higher energy orbital on the t-butyl radical than the beta space charge transfer.

contribution for the hydronium systems as the gap decreases. The charge transfer term likewise becomes more pronounced for the ammonium systems as the gap decreases; however, it does so not nearly as rapidly as in the hydronium case, which one might expect given the greater proton affinity of ammonia. The fact that classic perturbation theory arguments based on species in isolation are born out in the ALMO-EDA method for these simple systems highlights its physicality, and potential for application to more complicated systems where chemical intuition becomes strained.

A graphical representation of the data from COVP analysis of these systems appears in Fig. 3. The fact that most of the energy lowering is captured by one or two pairs for each spin indicates that the SVD of charge transfer amplitudes was successful in condensing the information about all occupied mixings with all virtuals into a small, conceptually tractable, number of pairwise interactions. It should be noted that the ordering of COVPs is based on the magnitude of the singular value and not the energy lowering, the two differing by the Fock matrix element in the COVP basis (cf. Eq. (28)). Figure 3 shows that most of the charge transfer energy lowering comes from orbital mixings where the occupied orbital is on the alkyl species and the virtual orbital is on one of the molecular cations while CT interactions with alkali cations are almost not existent. Donation by the alkyl species is chiefly in the alpha space when it is open shell (the alpha HOMO is higher in energy than the beta HOMO) and necessarily distributed equally among the alpha and beta spaces when the alkyl species is closed shell. Back bonding to the alkyl unit is minimal but becomes more pronounced in the more strongly binding systems and occurs primarily in the beta space (the beta LUMO is lower in energy).

Depictions of the most important complementary occupied virtual orbital pairs for the interaction of hydronium with radical $(CH_3)_3C^\bullet$ and closed shell $(CH_3)_3CH$ in both the alpha and beta spaces, appear in Fig. 4 along with their corresponding energy lowerings. In all cases, the orbitals are well aligned for overlap, and donation is to a σ^* like virtual orbital (mesh) on the hydronium. The interaction resembles traditional hydrogen bonding interactions in the closed shell case, but begins to resemble chemical bonding in the radical. In the case of hydronium interacting with $(CH_3)_3C^\bullet$, the occupied orbital (transparent) of the alpha COVP is considerably different from that of the beta COVP, which has one fewer node. This observation is consistent with the interpretation that, in the radical case, the primary donation to the molecular cation is from the higher energy alpha HOMO and that, because it is lower lying, the beta occupied orbital participates as a donor orbital to a lesser degree. Additionally, the nodal structure of the alpha occupied orbital for the radical species is similar to that of the closed shell species in both the alpha and beta spaces, as one might expect.

Polarization arises from the mixing of all occupied orbitals on a given fragment with all virtual orbitals on that same fragment. The strength of such mixings will generally be related to the HOMO LUMO gap within a fragment. The calculated intra-fragment gaps (beta) for the isolated,

undistorted geometries are 4.5, 8.6, 6.4, and 10.6 eV for $(CH_3)_3C^\bullet$, $(CH_3)_3CH$, $CH_3^\bullet$, and CH_4, respectively. The gaps for the (quite unpolarizable) isolated cations are noticeably higher: 20.6, 16.0, 32.1, and 12.7 eV for K^+, NH_4^+, Na^+, and H_3O^+, respectively. The degree of polarization additionally depends on the proximity of the other, perturbing species to the more polarizable unit. The degree of proximity (optimized complex geometry) in turn depends on all modes of interaction. Moreover, the geometry is complicated by the constraints imposed by steric interactions. Fortunately, steric considerations are fairly uniform across the complexes for a given alkyl fragment since the concern is primarily the accessibility of the central carbon (or its CH bond).

A plot of the polarization contribution versus the binding energy, the term that encapsulates all forms of interaction and thus the motivation for close interfragment distances, appears in Fig. 5. Also in the figure are linear fits showing a strong relationship between POL and E_{Bind} within alkyl fragment groupings. The accessibility of the central carbon is comparable between the two radical species; however, the slope for $(CH_3)_3C^\bullet$ is considerably greater than that for $CH_3^\bullet$, reflecting greater polarization per unit strength of interaction for the smaller gap $(CH_3)_3C^\bullet$. In the closed shell case, the hydrogen atom absent in the open shell case is most proximal to the perturbing species and thus critical to polarization; however, among the closed shell species, the ordering of slopes in Fig. 5 still matches the intra-fragment orbital gap ordering. It should be noted that the electronic structure of the isolated, undistorted fragments does not directly enter the ALMO calculation outside of the geometric distortion calculation. The ALMO EDA thus gives physically meaningful results commensurate with chemical intuition of isolated functional units (provided, as is true in this case, the identification of functional units is appropriate) and thus invites application to more opaque interactions.

Geometric distortion is quite large for the more strongly bonding hydronium systems particularly when a radical is involved and CT into the σ^* orbital, is substantial, causing the lengthening of the H–X bond. Most of the frozen orbital interactions in this set of systems are unfavorable, stemming in large part from strongly overlapping frozen occupied spaces that are highly repulsive and necessitate considerable density reorganization. Moreover, unfavorable frozen interactions are particularly prominent in structures with large charge transfer contributions as bringing atoms into close contact for better orbital overlap is often accompanied by increased core-core repulsions. It is interesting to note that the difference in interaction energy for the alkali cation species interacting with open shell as opposed to closed shell alkyl species is primarily due to the sign change of the frozen energy, which becomes favorable in the open shell case due to the lack of repulsion with the removed hydrogen.

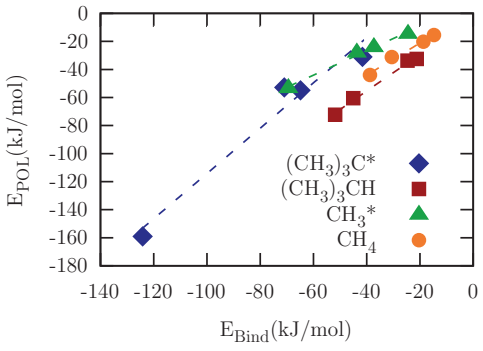

FIG. 5. E_{POL}(kJ/mol) Plotted Against E_{Bind}(kJ/mol) for Alkyl Systems: Grouping is by alkyl species for steric reasons. There is a strong linear relationship between polarization and E_{Bind}, which encapsulates the overall degree of interaction, within steric groupings. Additionally, within radical/closed shell categories, there is an inverse relationship between the slopes and the respective alkyl intrafragment orbital gaps (cf. text).

B. Benzene radical cation complexes

The strongly bound intermolecular systems involving benzene radical cations and nucleophiles are reminiscent of transition structures for nucleophilic aromatic substitution reactions.[47] Additionally, the benzene radical cation is sufficiently large to offer two binding sites that lead to noticeable differences in the character of the interaction even when the same species are involved (see below). For these reasons, we expand on the systems investigated both experimentally and theoretically by Mizuse *et al.*[47] to include not only different nucleophiles but also different orientations (local minima). The nucleophiles were chosen such that they spanned a large range of experimental[64] ionization potentials (IP) as these quantities were identified as important to explaining the geometric trends in terms of charge transfer in the original work.[47]

Table II contains the ALMO EDA data for these systems together with the experimental IP of the nucleophile. A graphical version of the EDA data for systems containing the aryl radical cation and a nucleophile appears in Fig. 6, and the corresponding COVP data appear in Fig. 7.

It is immediately apparent that a large range of binding energies is present; however, these binding energies only

TABLE II. Aryl Radical ALMO EDA Results: EDA terms (kJ/mol) and nucleophile Ionization Potentials (IP)[64] for systems containing the benzene radical cation and a nucleophile in the given orientation, on-top or side-on. Note, for on-top orientations, the erratic dependence of the total binding energy on nucleophile IP but nearly monotonic dependence of V-CT on the same quantity. The IP of benzene and thus the Electron Affinity (EA) of the aryl radical cation acceptor is 9.24 eV.[64]

Orientation	Nucleophile	GD	FRZ	POL	V-CT	Bind	IP (eV)
Top	PH_3	22.1	69.4	− 22.3	− 140.5	− 71.4	9.87
	NH_3	10.3	46.4	− 29.2	− 107.0	− 79.5	10.07
	CH_3COOH	27.2	− 18.1	− 20.3	− 46.7	− 57.9	10.65
	CH_3OH	3.8	7.7	− 15.1	− 45.4	− 49.0	10.84
	CH_3Cl	2.2	8.8	− 11.6	− 38.1	− 38.7	11.26
	HBr	2.1	26.2	− 5.1	− 46.2	− 23.0	11.68
	CH_3CN	1.4	− 19.9	− 17.3	− 22.8	− 58.6	12.20
	H_2O	0.7	− 11.1	− 7.9	− 17.0	− 35.3	12.62
Side	CH_3COOH	2.4	− 30.4	− 11.7	− 4.4	− 44.1	10.65
	CH_3OH	0.6	− 22.6	− 9.0	− 9.3	− 40.4	10.84
	CH_3CN	0.3	− 33.8	− 12.9	− 6.8	− 53.1	12.20
	H_2O	0.3	− 25.3	− 6.9	− 4.7	− 36.6	12.62

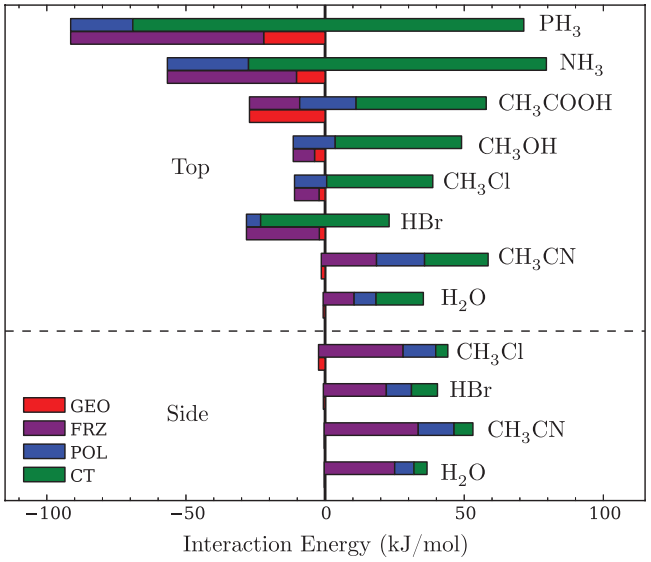

FIG. 6. Aryl Radical EDA Results: Unfavorable terms, such as geometric distortion are placed on the bottom of a double bar and grow to the left (negative). On the top bar, favorable terms such as polarization grow to the right (positive). By construction, the binding energy can then be read as the length of the bar to the right. Notice the considerable shift toward dependence on frozen interactions rather than charge transfer when a species is oriented on the side rather than on top and also the very similar binding energy for water in the two orientations despite the considerably different character of interaction.

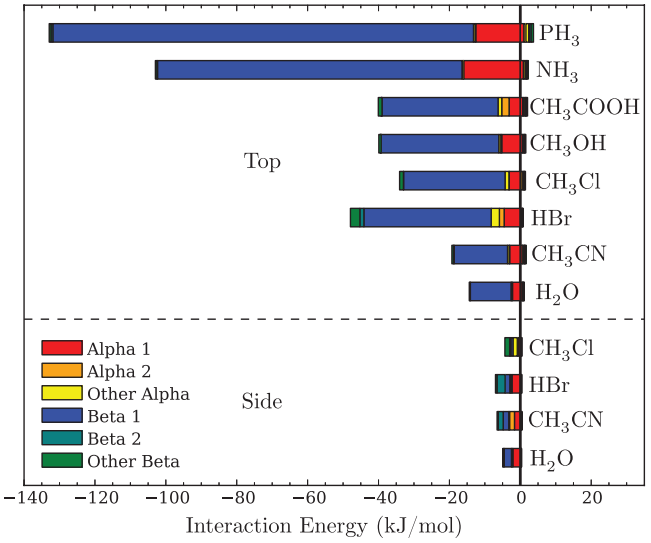

FIG. 7. Aryl Radical COVP Results: All interactions are favorable, and the direction of growth from zero indicates the directionality of the charge transfer. Energy contributions to the left of zero involve COVPs with the acceptor orbital on the aryl radical cation species while those on the right correspond to charge donation to the nucleophile. Contributions from orbital interactions in the alpha space are denoted with warm colors and those in the beta space with cool colors to facilitate the recognition of symmetry or asymmetry with respect to spin. Each color indicates a different occupied-virtual orbital pair's energy contribution. Additionally, the total length of the bar indicates the magnitude of the charge transfer energy lowering calculated by perturbation theory. Charge transfer is primarily from the nucleophile to the electron deficient aryl radical cation and, for on-top systems, in the beta space as the radical has a lower-lying beta LUMO accessible in that orientations. Charge transfer is diminished for side-on systems but largely symmetric with respect to spin due to poor overlap with the low-lying beta orbital.

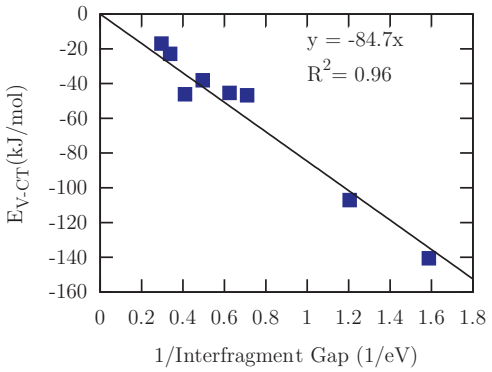

FIG. 8. $E_{\text{V-CT}}$(kJ/mol) Plotted Against the Inverse of the Interfragment Orbital Energy Gap (eV; IP of nucleophile less IP of benzene): Data are for systems containing the aryl radical cation and on-top oriented nucleophile. The equation is of the form $E_{\text{V-CT}} = a/\text{Gap}$; a = −84.7 kJ eV/mol, the accurate fit demonstrates the consistency of the ALMO V-CT term with a perturbation theory understanding of orbital interactions based on isolated species. Minimal error in the fit was incurred by forcing the physically meaningful zero intercept.

correlate roughly with ionization potential. The electron affinity of the benzene radical cation can be taken as equivalent to the ionization potential of benzene, 9.24 eV,[64] and the difference between the nucleophile IP and the benzene IP can then be considered the inter-fragment orbital energy gap. A plot of the charge transfer contribution to the binding energy versus one over the inter-fragment gap for systems with an on-top orientation appears in Fig. 8. The linear fit indicates a strong correlation and reaffirms the connection between the ALMO charge transfer term and the long standing perturbation arguments made to explain orbital interactions. Again it should be noted that this connection arises naturally rather than explicitly by construction. Indeed, while the ALMO CT contribution can be calculated perturbatively, the perturbative correction is carried out using the orbitals and Fock matrix resulting from the self-consistent polarization of the fragments, which, in the case of strongly interacting species such as these, are considerably different from their "frozen" counterparts determined completely by the calculation of the species in isolation. This observation thus argues again for the physicality of the charge transfer term in the ALMO EDA.

It should be no surprise that the smallest intra-fragment gap is that of the benzene radical cation in the beta space (2.04 eV; undistorted). Steric limitations to orientation are uniformly minimal across the systems considered in this section. Thus, by the same arguments made above, the polarization should largely depend on how strongly the nucleophile is able to interact with the aryl cation because this determines how closely the nucleophile is able to approach. This degree of interaction is once more taken to be encapsulated in the total binding energy of the system, and the plot of polarization energy versus total binding energy. Figure 9 again shows a relatively strong linear relationship between the two quantities despite the diversity of nucleophiles and orientations.

Because there are few other atoms hindering the approach of the two species, the most significant core-core repulsions should arise as a consequence of maximizing overlap for donor acceptor orbital interactions. Additionally, systems

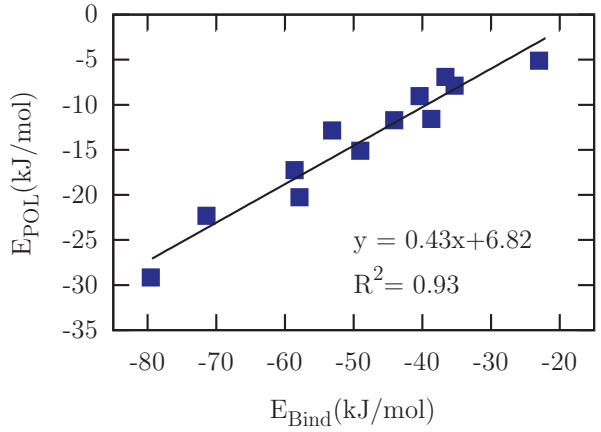

FIG. 9. E_{POL}(kJ/mol) Plotted Against E_{Bind}(kJ/mol) for All Aryl Radical Cation Systems. All nucleophiles and orientations considered in this work are included. All systems are included in a single fit because the species with the smallest intrafragment orbital energy gap is in all cases the aryl radical cation and because steric concerns are fairly uniform. The fairly accurate fit despite the diversity of systems reaffirms the interpretation and strong physical content of the ALMO polarization term.

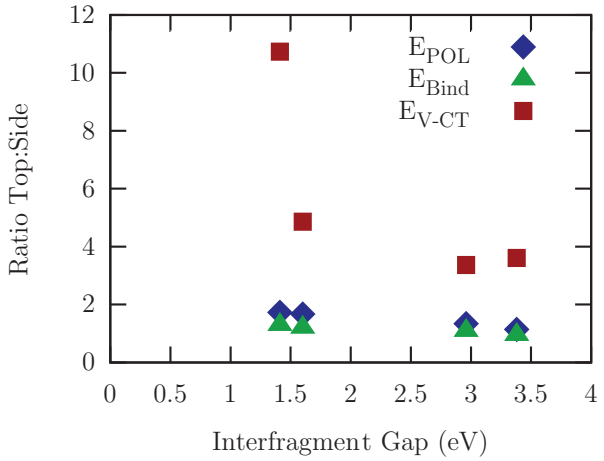

FIG. 11. The Ratio (Top:Side) of the E_{V-CT}, E_{POL}, and E_{Bind} Contributions Plotted Against IP(eV): Systems shown are those with both an on-top and a side-on structure. This plot shows the considerable shift toward dependence on charge transfer interactions as IP decreases toward that of benzene (9.24 eV) when going from side-on to on-top orientation. The top:side ratio for E_{POL} increases for smaller interfragment orbital energy gaps because of the closer contacts. These close contacts are brought about by the potential for energetically attractive orbital interactions and introduce a stronger perturbation for intramolecular mixings. The E_{POL} ratio increases more slowly than that for E_{V-CT}, and that for E_{Bind} increases even more slowly because of the unfavorable frozen interactions incurred by the closer approach of the species.

that do not have strong core-core repulsions should have fairly favorable frozen orbital energy contributions as the interaction is, after all, between a cation and one of several neutral molecules with considerable dipole moments. Indeed, the plot of V-CT versus FRZ, Fig. 10, for all super-molecular complexes containing the aryl radical cation, irrespective of nucleophile orientation, shows a fairly strong linear correlation despite the variety of systems.

It has been shown that smaller inter-fragment gaps generally lead to more charge transfer; however, these dative interactions can only take place if there is sufficient overlap of the relevant orbitals, as is the case for the top oriented species. A plot of the ratio of charge transfer in the top oriented complex to that of the side oriented complex for the same fragment pairs appears in Fig. 11. The plot shows that, for smaller interfragment gaps, the shift to increased charge transfer when going from the side to the top orientation is dramatically more

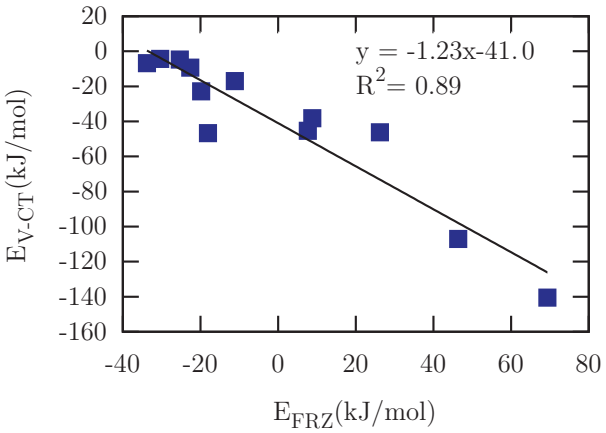

FIG. 10. E_{V-CT}(kJ/mol) Plotted Against E_{FRZ}(kJ/mol) for all Aryl Radical Cation Systems. All nucleophiles and orientations considered in this work are included. The linear correlation demonstrates the origin of the unfavorable Frozen interaction terms for these systems: core-core and exchange interactions resulting from close proximity needed for improved orbital overlap.

pronounced. Additionally, the analogous plots for E_{Bind} and E_{POL} in Fig. 11 show that, for smaller inter-fragment gaps, the ratio of binding energies increases though not as quickly as does the ratio of polarization energy contributions and neither as quickly as the charge transfer contribution. These findings together indicate a considerable shift toward stronger binding through enhanced dative interactions when orbitals are favorably aligned and considerably more emphasis on polarization and frozen interactions (by subtraction) when orbital alignment is not optimal.

COVP analysis of the aryl radical cation complexes, Fig. 7 shows that the charge transfer energy lowering is due to mixings between occupied donor orbitals on the nucleophile and virtual acceptor orbitals on the aryl radical cation with negligible backbonding. These mixings are primarily in the beta space for the top oriented geometries in which the nucleophile donor orbital is well aligned with the low-lying beta LUMO of the aryl radical cation. Alternatively, the side orientations exhibit charge transfer that is quite symmetric with respect to alpha and beta despite the radical nature of the species involved, simply because the half-occupied benzene hole orbital is inaccessible.

While the binding energy of the water and aryl radical cation system is almost the same for both top and side orientations, the ALMO EDA reveals considerably different modes of interaction in the two cases. The side interaction is dominated by frozen orbital contributions while the interaction in the top orientation is more noticeably charge transfer in character (cf. Fig. 6). The most important COVPs for the interaction of the aryl radical cation with water in both top and side orientations are displayed along with their corresponding energy lowering in Fig. 12. These orbital plots show that the beta donation for the top case is into a π orbital which,

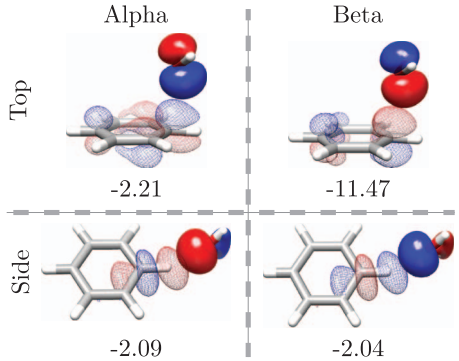

FIG. 12. Representative COVP Images for Aryl Radical Cation Systems: The most important COVPs in the alpha and beta spaces for the interaction of water with the benzene radical cation in both the on-top and side-on orientations. The charge transfer energy lowering (kJ/mol) associated with each orbital pair is also shown. The virtual (acceptor) orbital of the pair is depicted as a mesh isosurface while that for the occupied (donor) orbital is represented with a translucent isosurface. For the side case, charge transfer is roughly symmetric with respect to spin and primarily into a C–H σ^* orbital on the aryl radical cation. For the top case, charge transfer is from a lone pair orbital on water into a somewhat localized π orbital on the aryl radical cation. In the beta space, this acceptor orbital has one fewer node (lower energy) and thus leads to greater energy lowering.

as confirmed by the number of nodes, is lower in energy than the acceptor orbital in the alpha space, leading to the asymmetry with respect to spin in the energy lowerings. Conversely, charge donation for the side orientation is into the C–H σ^* orbital, which is very similar for both spins, and the energy lowering is roughly symmetric. The donor orbital in all cases is a non-bonding lone pair orbital on the water.

It should be noted that the β acceptor orbital does not closely resemble the benzene HOMO, because the COVP reflects the optimal compromise between large numerator (good orbital interaction) and small denominator (energy gap) to most compactly describe the interaction. Thus the β acceptor orbital also contains contributions from other, higher, empty π levels to enable spatial localization.

V. CONCLUSIONS

The ALMO EDA has been successfully extended to open shell systems, and applied to two classes of examples. While these open shell interactions are considerably stronger than many closed shell intermolecular interactions, the ALMO-EDA continues to yield physically meaningful results. Two examples identified herein include polarization contributions that depend on the intra-fragment gap, and inter-fragment charge transfer interactions that depend on the inter-fragment orbital gap. Moreover, the ALMO EDA and COVP analysis were also able to distinguish two different interactions involving the same species, water and the aryl radical cation, with similar overall binding energies. Thus the ALMO-EDA can be useful to explore and distinguish seemingly equivalent binding sites within a given model chemistry. Here it should be noted that the ALMO EDA is contingent on the model chemistry's accurate portrayal of all relevant interactions (e.g., exchange, correlation, and dispersion).

The application of the ALMO EDA to the alkane/alkyl radical interactions with cations, and benzene cation interacting with nucleophiles has also served to illustrate some general features of open shell intermolecular interactions. First, while orbital interactions (CT) can be very important, they do depend on proper intermolecular overlap of relevant orbitals. For alkyl radicals interacting with alkali cations, CT is very small because there are no energetically relevant acceptor orbitals. Similarly nucleophiles interacted with benzene cation by other means when intermolecular orbital overlap for the most energetically relevant orbitals was poor (side-on complexes).

A second observation is that strongly unfavorable frozen interactions are typically accompanied by considerable charge transfer energy lowering. Although polarization terms are also large for systems where frozen interactions are considerably unfavorable (because fragments are close and the perturbation causing intra-fragment mixings is large) the real driving force for the close inter-fragment separations that can occur in open shell systems seems to be better orbital overlaps for charge transfer interactions. The increased polarization energy lowering largely serves to mitigate the high energetic cost incurred by the closer approach. Closer approach becomes unhelpful for overall interaction strength more rapidly when the means of lowering the system energy are restricted to polarization alone.

It is our view that there is much still to be done in unravelling intermolecular interactions, particularly when open shell fragments are involved. For instance, we intend to investigate the effects of the exclusion of different modes of interaction on the super-molecular structure so as to disentangle the considerable dependence of intermediate state energies on the ultimate geometry. Additionally, while the results of the ALMO EDA are both physically reasonable and insightful, it is of interest to explore strict bounds on physically meaningful contributions so as to refine quantitative definitions of interactions in a subfield that can often be quite qualitative.

ACKNOWLEDGMENTS

We would like to thank Professor Hammerum for some of the geometries used in this study. This work was supported by the Director, Office of Science, Office of Basic Energy Sciences of the U.S. Department of Energy under Contract No. DE-AC02-05CH11231 at Lawrence Berkeley National Laboratory. We also acknowledge computational resources obtained under NSF Award No. CHE-1048789.

[1]S. Rybak, B. Jeziorski, and K. Szalewicz, "Many-body symmetry-adapted perturbation theory of intermolecular," J. Chem. Phys. **95**(9), 6576 (1991).
[2]B. Jeziorski, R. Moszynski, and K. Szalewicz, "Perturbation theory approach to intermolecular potential energy surfaces of van der Waals complexes," Chem. Rev. **94**(7), 1887 (1994).
[3]W. H. Adams, "Two new symmetry-adapted perturbation theories for the calculation of intermolecular interaction energies," Theor. Chem. Acc. **108**, 225–231 (2002).
[4]A. Misquitta, B. Jeziorski, and K. Szalewicz, "Dispersion energy from density-functional theory description of monomers," Phys. Rev. Lett. **91**(3), 033201 (2003).

[5]A. J. Misquitta, R. Podeszwa, B. Jeziorski, and K. Szalewicz, "Intermolecular potentials based on symmetry-adapted perturbation theory with dispersion energies from time-dependent density-functional calculations," J. Chem. Phys. **123**, 214103 (2005).

[6]P. S. Żuchowski, R. Podeszwa, R. Moszyski, B. Jeziorski, and K. Szalewicz, "Symmetry-adapted perturbation theory utilizing density functional description of monomers for high-spin open-shell complexes," J. Chem. Phys. **129**, 084101 (2008).

[7]A. J. Stone and A. J. Misquitta, "Charge-transfer in symmetry-adapted perturbation theory," Chem. Phys. Lett. **473**, 201–205 (2009).

[8]M. Hapka, P. S. Żuchowski, M. M. Szczniak, G. Chaasiski, "Symmetry-adapted perturbation theory based on unrestricted Kohn-Sham orbitals for high-spin open-shell van der Waals complexes," J. Chem. Phys. **137**, 164104 (2012).

[9]E. G. Hohenstein and C. David Sherrill, "Wavefunction methods for noncovalent interactions," WIREs Comput. Mol. Sci. **2**, 304–326 (2012).

[10]K. U. Lao and J. M. Herbert, "Accurate intermolecular interactions at dramatically reduced cost: XPol+SAPT with empirical dispersion," J. Phys. Chem. Lett. **3**, 3241–3248 (2012).

[11]K. Szalewicz, "Symmetry-adapted perturbation theory of intermolecular forces," WIREs Comput. Mol. Sci. **2**, 254–272 (2012).

[12]M. S. Gordon, M. A. Freitag, P. Bandyopadhyay, J. H. Jensen, V. Kairys, and W. J. Stevens, "The effective fragment potential method: A QM-based MM approach to modeling," J. Phys. Chem. A **105**(2), 293 (2001).

[13]I. Adamovic, M. A. Freitag, and M. S. Gordon, "Density functional theory based effective fragment potential method," J. Chem. Phys. **118**(15), 6725 (2003).

[14]H. Li, M. S. Gordon, and J. H. Jensen, "Charge transfer interaction in the effective fragment potential method," J. Chem. Phys. **124**, 214108 (2006).

[15]M. S. Gordon, J. M. Mullin, S. R. Pruitt, L. B. Roskop, L. V. Slipchenko, and J. A. Boatz, "Accurate methods for large molecular systems," J. Phys. Chem. B **113**(29), 9646–9663 (2009).

[16]E. D. Glendening and A. Streitwieser, "Natural energy decomposition analysis: An energy partitioning procedure for molecular interactions with application to weak hydrogen bonding, strong ionic, and moderate donor-acceptor interactions," J. Chem. Phys. **100**(4), 2900–2909 (1994).

[17]G. K. Schenter and E. D. Glendening, "Natural energy decomposition analysis: The linear response electrical self energy," J. Phys. Chem. **100**(43), 17152–17156 (1996).

[18]E. D. Glendening, "Natural energy decomposition analysis: extension to density functional methods and analysis of cooperative effects in water clusters," J. Phys. Chem. A **109**(51), 11936–11940 (2005).

[19]A. E. Reed, L. A. Curtiss, and F. Weinhold, "Intermolecular interactions from a natural bond orbital, donor-acceptor viewpoint," Chem. Rev. **88**, 899–926 (1988).

[20]K. Kitaura and K. Morokuma, "A new energy decomposition scheme for molecular interactions within the Hartree-Fock approximation," Int. J. Quantum Chem. **10**, 325–340 (1976).

[21]T. Ziegler and A. Rauk, "On the calculation of bonding energies by the Hartree Fock slater method," Theor. Chim. Acta **46**, 1–10 (1977).

[22]T. Ziegler and A. Rauk, "A theoretical study of the ethylene-metal bond in complexes between Cu+, Ag+, Pt0, or Pt2+ and ethylene, based on Hartree-Fock-Slater transition-state method," Inorg. Chem. **18**(6), 1558–1565 (1979).

[23]M. P. Mitoraj, A. Michalak, and T. Ziegler, "A combined charge and energy decomposition scheme for bond analysis," J. Chem. Theory Comput. **5**(4), 962–975 (2009).

[24]P. S. Bagus, K. Hermann, and C. W. Bauschlicher, Jr., "A new analysis of charge transfer and polarization for ligand-metal bonding: Model studies of AI4 CO and AI4NH3," J. Chem. Phys. **80**(9), 4378 (1984).

[25]W. J. Stevens and W. H. Fink, "Frozen fragment reduced variational space analysis of hydrogen bonding interactions. Application to the water dimer," Chem. Phys. Lett. **139**(1), 15–22 (1987).

[26]F. M. Bickelhaupt and E. J. Baerends, "Kohn-Sham density functional theory: Predicting and understanding chemistry," Rev. Comput. Chem. **15**, 1 (2000).

[27]P. Su and H. Li, "Energy decomposition analysis of covalent bonds and intermolecular interactions," J. Chem. Phys. **131**, 014102 (2009).

[28]Y. Mo, J. Gao, and S. D. Peyerimhoff, "Energy decomposition analysis of intermolecular interactions using a block-localized wave function approach," J. Chem. Phys. **112**(13), 5530 (2000).

[29]R. Z. Khaliullin, M. Head-Gordon, and A. T. Bell, "An efficient self-consistent field method for large systems of weakly interacting components," J. Chem. Phys. **124**, 204105 (2006).

[30]Y. Mo, L. Song, and Y. Lin, "Block-localized wavefunction (BLW) method at the density functional theory (DFT) level," J. Phys. Chem. A **111**, 8291–8301 (2007).

[31]Y. Mo, P. Bao, and J. Gao, "Energy decomposition analysis based on a block-localized wavefunction and multistate density functional theory," Phys. Chem. Chem. Phys. **13**, 6760–6775 (2011).

[32]S. N. Steinmann, C. Corminboeuf, W. Wu, and Y. Mo, "Dispersion-corrected energy decomposition analysis for intermolecular interactions based on the BLW and dDXDM methods," J. Phys. Chem. A **115**, 5467–5477 (2011).

[33]A. J. Sadlej, "Long range induction and dispersion interactions between Hartree-Fock subsystems," Mol. Phys. **39**, 1249–1264 (1980).

[34]Q. Wu, P. W. Ayers, and Y. Zhang, "Density-based energy decomposition analysis for intermolecular interactions with variationally determined intermediate state energies," J. Chem. Phys. **131**, 164112 (2009).

[35]M. H. Cohen, A. Wasserman, R. Car, and K. Burke, "Charge transfer in partition theory," J. Phys. Chem. A **113**(10), 2183–2192 (2009).

[36]P. Elliott, K. Burke, M. H. Cohen, and A. Wasserman, "Partition density-functional theory," Phys. Rev. A **82**, 024501 (2010).

[37]R. Z. Khaliullin, E. A. Cobar, R. C. Lochan, A. T. Bell, and M. Head-Gordon, "Unravelling the origin of intermolecular interactions using absolutely localized molecular orbitals," J. Phys. Chem. A **111**(36), 8753–8765 (2007).

[38]R. Z. Khaliullin, A. T. Bell, and M. Head-Gordon, "Analysis of charge transfer effects in molecular complexes based on absolutely localized molecular orbitals," J. Chem. Phys. **128**, 184112 (2008).

[39]E. A. Cobar, P. R. Horn, R. G. Bergman, and M. Head-Gordon, "Examination of the hydrogen-bonding networks in small water clusters (n = 2–5, 13, 17) using absolutely localized molecular orbital energy decomposition analysis," Phys. Chem. Chem. Phys. **14**, 15328–15339 (2012).

[40]J. M. J. Swanson and J. Simons, "Role of charge transfer in the structure and dynamics of the hydrated proton," J. Phys. Chem. B **113**(15), 5149–5161 (2009).

[41]D. H. Ess, S. M. Bischof, J. Oxgaard, R. A. Periana, and W. A. Goddard, "Transition state energy decomposition study of acetate-assisted and internal electrophilic substitution C-H bond activation by (acac-O, O) 2 Ir (X) Complexes (X) CH3 COO, OH)," Organometallics **27**, 6440–6445 (2008).

[42]D. H. Ess, W. A. Goddard, and R. A. Periana, "Electrophilic, ambiphilic, and nucleophilic CH bond activation: Understanding the electronic continuum of CH bond activation through transition-state and reaction pathway interaction energy decompositions," Organometallics **29**(23), 6459–6472 (2010).

[43]D. S. Lambrecht, G. N. I. Clark, T. Head-Gordon, and M. Head-Gordon, "Exploring the rich energy landscape of sulfate-water clusters SO4(2–)(H2O)(n = 3–7): an electronic structure approach," J. Phys. Chem. A **115**, 11438–11454 (2011).

[44]E. Ramos-Cordoba, D. S. Lambrecht, and M. Head-Gordon, "Charge-transfer and the hydrogen bond: Spectroscopic and structural implications from electronic structure calculations," Faraday Discuss. **150**, 345 (2011).

[45]R. M. Young, R. Julian Azar, M. A. Yandell, S. B. King, M. Head, and D. M. Neumark, "Iodide solvation in tetrahydrofuran clusters: $I^-(THF)_n$ ($1 \leq n \leq 30$)," Mol. Phys. **110**(15–16), 1787–1799 (2012).

[46]S. Hammerum, "Alkyl radicals as hydrogen bond acceptors: computational evidence," J. Am. Chem. Soc. **131**(24), 8627–8635 (2009).

[47]K. Mizuse, H. Hasegawa, N. Mikami, and A. Fujii, "Infrared and electronic spectroscopy of benzene-ammonia cluster radical cations [C(6)H(6)(NH(3))(1,2)](+): observation of isolated and microsolvated σ-complexes," J. Phys. Chem. A **114**(42), 11060–11069 (2010).

[48]M. Head-Gordon, P. E. Maslen, and C. A. White, "A tensor formulation of many-electron theory in a nonorthogonal single-particle basis," J. Chem. Phys. **108**, 616–625 (1998).

[49]H. Stoll, G. Wagenblast, and H. Preuß, "On the use of local basis sets for localized molecular orbitals," Theor. Chim. Acta **57**, 169–178 (1980).

[50]E. Gianinetti, M. Raimondi, and E. Tornaghi, "Modification of the Roothaan equation to exclude BSSE from molecular interaction calculations," Int. J. Quantum Chem. **60**, 157–166 (1996).

[51]E. Gianinetti, I. Vandoni, A. Famulari, and M. Raimondi, "Extension of the SCF-MI method to the case of K fragments one of which is an open-shell system," Adv. Quantum Chem. **31**, 251–266 (1998).
[52]P. Pulay, "Improved SCF convergence acceleration," J. Comput. Chem. **3**(4), 556–560 (1982).
[53]W. Z. Liang and M. Head-Gordon, "Approaching the basis set limit in density functional theory calculations using dual basis sets without diagonalization," J. Phys. Chem. A **108**(15), 3206–3210 (2004).
[54]R. Azar, P. R. Horn, E. J. Sundstrom, and M. Head-Gordon, "Useful lower limits to polarization contributions to intermolecular interactions using a minimal basis of localized orthogonal orbitals: Theory and analysis of the water dimer," J. Chem. Phys. **138**, 084102 (2013).
[55]See supplementary material at http://dx.doi.org/10.1063/1.4798224 for geometries and for energies with different basis sets and functionals.
[56]S. Grimme, "Semiempirical GGA-type density functional constructed with a long-range dispersion correction," J. Comput. Chem. **27**, 1787–1799 (2006).
[57]Y. Shao, L. Fusti Molnar, Y. Jung, J. Kussmann, C. Ochsenfeld, S. T. Brown, A. T. B. Gilbert, L. V. Slipchenko, S. V. Levchenko, D. P. O'Neill, R. A. DiStasio, R. C. Lochan, T. Wang, G. J. O. Beran, N. A. Besley, J. M. Herbert, C. Y. Lin, T. Van Voorhis, S. H. Chien, A. Sodt, R. P. Steele, V. A. Rassolov, P. E. Maslen, P. P. Korambath, R. D. Adamson, B. Austin, J. Baker, E. F. C. Byrd, H. Dachsel, R. J. Doerksen, A. Dreuw, B. D. Dunietz, A. D. Dutoi, T. R. Furlani, S. R. Gwaltney, A. Heyden, S. Hirata, C.-P. Hsu, G. Kedziora, R. Z. Khalliulin, P. Klunzinger, A. M. Lee, M. S. Lee, W. Liang, I. Lotan, N. Nair, B. Peters, E. I. Proynov, P. A. Pieniazek, Y. M. Rhee, J. Ritchie, E. Rosta, C. David Sherrill, A. C. Simmonett, J. E. Subotnik, H. Lee Woodcock, W. Zhang, A. T. Bell, A. K. Chakraborty, D. M. Chipman, F. J. Keil, A. Warshel, W. J. Hehre, H. F. Schaefer, J. Kong, A. I. Krylov, P. M. W. Gill, and M. Head-Gordon, "Advances in methods and algorithms in a modern quantum chemistry program package," Phys. Chem. Chem. Phys. **8**(27), 3172–3191 (2006).
[58]A. D. Becke, J. Chem. Phys. **98**, 5648–5652 (1993).
[59]J.-D. Chai and M. Head-Gordon, J. Chem. Phys. **128**, 084106 (2008).
[60]J.-D. Chai and M. Head-Gordon, Phys. Chem. Chem. Phys. **10**, 6615–6620 (2008).
[61]Y. Zhao and D. Truhlar, Theor. Chem. Acc. **120**, 215–241 (2008).
[62]E. F. Pettersen, T. D. Goddard, C. C. Huang, G. S. Couch, D. M. Greenblatt, E. C. Meng, and T. E. Ferrin, "UCSF Chimera–a visualization system for exploratory research and analysis," J. Comput. Chem. **25**(13), 1605–1612 (2004).
[63]S. Hammerum and C. B. Nielsen, "Intramolecular hydrogen bonding and hydrogen atom abstraction in gas-phase aliphatic amine radical cations," J. Phys. Chem. A **109**(51), 12046–12053 (2005).
[64]S. G. Lias, J. E. Bartmess, J. F. Liebman, J. L. Holmes, R. D. Levin, and W. G. Mallard, "Ion Energetics Data" in *NIST Chemistry WebBook, NIST Standard Reference Database Number 69*, edited by P. J. Linstrom and W. G. Mallard (National Institute of Standards and Technology, Gaithersburg, MD, 2011), http://webbook.nist.gov (retrieved December 25, 2012).